Structure and phases of the Au(001) surface: X-ray scattering measurements

D. M. Zehner
Solid State Division, Oak Ridge National Laboratory, Oak Ridge, Tennessee 37831

S. G. J. Mochrie
Physics Department, Massachusetts Institute of Technology, Cambridge, Massachusetts 02139

B. M. Ocko and Doon Gibbs
Physics Department, Brookhaven National Laboratory, Upton, New York 11973

(Received 15 October 1990; accepted 17 December 1990)

X-ray diffraction is used to study the phase behavior and structure of the Au(001) surface between 300 K and the triple point. For $T > 1170$ K, the x-ray reflectivity is consistent with a thin, disordered surface film. At $T = 1170$ K, there is a reversible transition to an incommensurate, hexagonal overlayer that resides on top of the square substrate. At 970 K, the orientation of the hexagonal layer rotates discontinuously by 0.81° with no observable change in incommensurability.

I. INTRODUCTION

The Au(001) surface exhibits a novel reconstruction in which the topmost layer of atoms is believed to form a hexagonal lattice on top of planes of square symmetry lying immediately beneath. In spite of this appealingly simple picture, a completely consistent description of the room-temperature structure has yet to emerge.[1-5] Much less is known about the behavior at higher temperatures,[6] but one may anticipate that a temperature-dependent study of this surface will provide insights into two-dimensional structures and phase transitions. In addition, experiments at temperatures near bulk melting are essential for an understanding of the global stability of crystal surfaces, and of the relationships between such phenomena as roughening transitions, enhanced surface vibrations, and surface and bulk melting. Accordingly, we have carried out a comprehensive x-ray diffraction study of the clean Au(001) surface between 300 K and just below the triple point ($T_t = 1337$ K). Our results encompass a variety of behavior, including a rotational transition and a surface-disordering transition.[6-9] They also provide a detailed three-dimensional description of the surface structure.

In this paper, we discuss the results of glancing incidence, specular, and nonspecular x-ray reflectivity studies. In the glancing-incidence geometry, the incident and exit x-ray angles typically fall within a degree of the critical angle for total external reflection ($\alpha_c = 0.63°$ for Au at a wavelength of $\lambda \approx 1.7$ Å). This geometry is convenient for quantitative investigations of in-plane surface structure because contributions to the background are small, as a result of the small x-ray penetration depth. In the reflectivity studies, the incident and exit angles may increase to 45°, or larger. As will become apparent, this geometry is useful for characterizing the structure of the top and succeeding layers along the direction of the surface normal.

Experiments on the clean Au(001) surface, performed in an ultrahigh vacuum environment,[6-9] were carried out at beam line A2 at the Cornell High Energy Synchrotron Source and at the National Synchrotron Light Source using beam lines X22C, X20C, and X22B. For large incidence angles (α), slits were used to define the illuminated sample area and all scattered x rays were collected. Then, the reflectivity from a given surface periodicity ($\tau_x \tau_y$) is[6-9]

$$R = \left(\frac{4\pi r_0}{c^2 k \sin\alpha} 2\right) |F(Q)|^2 e^{-2W(Q)} \left| \sum_{n=0}^{\infty} \rho_Q(n) e^{iQ_z cn/2} \right|^2, \tag{1}$$

where $Q = k - k' = (\tau_x, \tau_y, Q_z)$ is the wave-vector transfer, r_0 is the Thomson radius, $F(Q)$ is the form factor, $W(Q)$ is the Debye–Waller factor, c is the cubic lattice constant of Au, and $\rho_Q(n)$ is the amplitude of the density wave in the nth layer. We will discuss specific forms for $\rho_Q(n)$ below. However, it is important to note that R is not sensitive to instrumental parameters, so that absolute measurements are possible. At grazing incidence, a Ge(111) analyzer was employed for fine resolution measurements of the overlayer lattice constants and rotation angle. A complete discussion of the sample preparation and characterization procedures has been given in Ref. 8.

Briefly, we have identified three distinct structural phases, which are exhibited by the Au(001) surface between $T = 300$ K and the bulk melting transition at $T = 1337$ K. They are (1) disordered ($1170 < T < 1320$ K), (2) distorted-hexagonal ($970 < T < 1170$ K), and (3) rotated, distorted-hexagonal ($300 < T < 970$ K). The symmetries of the diffraction patterns for these phases are shown in Fig. 1, where the data obtained in the glancing-incidence geometry are summarized. In the figure, each symbol represents a rod of scattering extending normal to the (001) planes. The rod scattering through the origin of reciprocal space is the specular reflectivity, while the off-axis rod scattering is the nonspecular reflectivity.

The diffraction pattern observed in the high-temperature phase between $T = 1170$ and 1337 K is shown in Fig. 1(a). Solid squares are indexed in bulk-cubic reciprocal-lattice units $(H, K, L)c$ and represent the reflectivity along directions normal to the surface joining all the bulk Bragg reflections. In the literature, these rods are referred to as crystal-truncation rods.[10] Thus the area enclosed by the solid

 0734-2101/91/031861-07$01.00

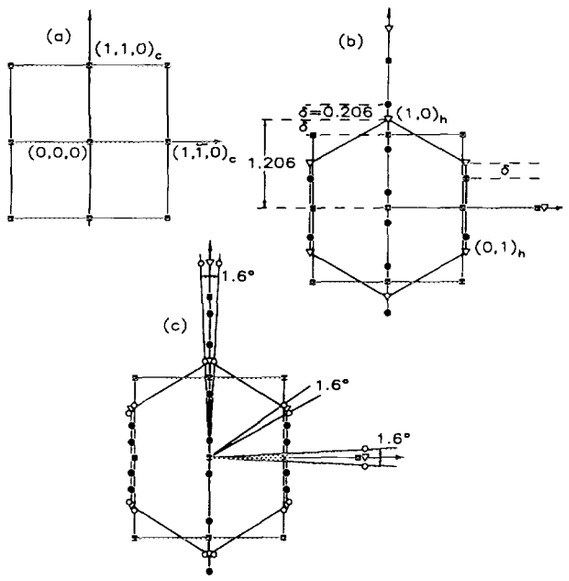

FIG. 1. In-plane diffraction pattern (H, K, 0.07) for the (001)c surface of Au. (a) Disordered phase, (b) distorted-hexagonal phase, and (c) rotated, distorted-hexagonal phase. Each point represents a rod of scattering extending normal to the surface. Bulk [110]c and [1$\bar{1}$0]c directions are indicated. Peaks corresponding to domains rotated by 90° were observed, but are not shown. All the data represented in this figure were obtained at fixed L = 0.07 in bulk reciprocal-lattice units.

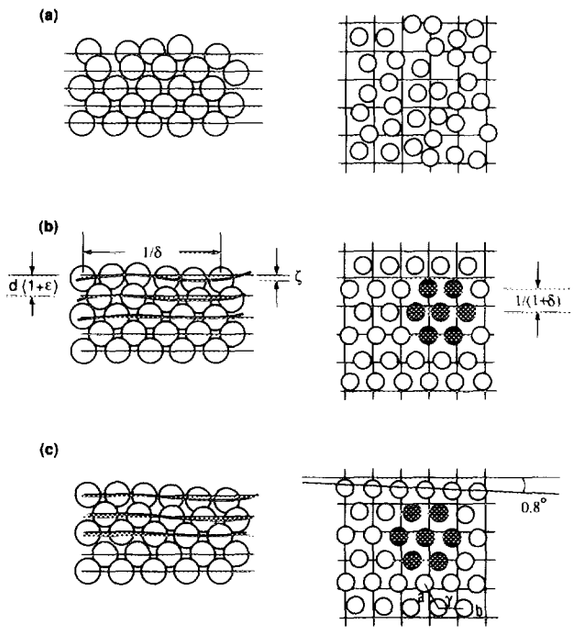

FIG. 2. Schematic real space side (left) and top (right) views of the observed phases of the Au (001), surface. (a) Disordered phase, (b) distorted-hexagonal phase, (c) rotated, distorted hexagonal. On the left is depicted the kind of information learned in reflectivity measurements, while on the right is the kind obtained at glancing incidence. ζ is the corrugation amplitude, δ is the incommensurability, d is the interlayer spacing of the ideally terminated bulk, and ϵ is the fractional change in interlayer spacing upon surface relaxation.

squares corresponds to the substrate unit cell. At elevated temperatures the in-plane diffraction pattern has the (1×1) symmetry of the bulk, consistent with an unreconstructed or disordered surface layer. More importantly, the Q_z dependence of the reflectivity is consistent with the existence of a thin disordered film (1–2 layers thick), and not with an ideally terminated crystal. Schematic real space side and top views of this phase of the Au(001) surface are shown in Fig. 2(a).

Below $T = 1170$ K there is a reversible transition to an incommensurate, two-dimensional structure of hexagonal symmetry. Hexagonal reciprocal-lattice vectors $(1, 0)h$ and $(0, 1)h$ are indicated by open triangles in Fig. 1(b). An important feature of this structure is an incommensurate corrugation along the cubic [110] direction with a wave vector (δ) just equal to the difference between overlayer $(1, 0)h$ and substrate $(1, 1, 0)c$ wave vectors. In Au reciprocal-lattice units, $\delta = (0.206 \pm 0.001)\sqrt{2}c^*$ ($c^* = 2\pi/c$, where $c = 4.08$Å at 300 K). This gives rise to satellites (solid circles) along directions parallel to the [110] direction, about each hexagonal position. The existence of the satellites at 300 K led to earlier descriptions of the surface as having a (5×1) reconstruction. As shown below, these satellites arise from modulations of the surface layer by the underlying square lattice, and vice versa. Real space schematic views of this phase, which we call the distorted-hexagonal phase, are shown in Fig. 2(b). The incommensurability in the [1$\bar{1}$0] direction is $(0.043 \pm 0.001)\sqrt{2}c^*$, but there are no corresponding satellite peaks.

Below $T = 970$ K, additional rods appear around each of the hexagonal rods, as shown by the open circles in Fig. 1(c). These occur at a fixed angle equal to $\pm 0.81°$, and reveal the existence of rotated domains (in coexistence with the aligned domains). In addition, higher harmonics are visible along the [110] direction [solids circles, Fig. 1(c)]. The transition to the rotated, distorted-hexagonal phase is reversible. It is surprising, when compared to the behavior of rare-gas adsorbates on graphite,[11–13] that the rotation angle and the incommensurability are observed to be only weakly temperature dependent between $T = 970$ and 300 K. Nevertheless, important features of the line shapes below $T = 970$ K depend sensitively on temperature and on sample history. For example, the correlation lengths are resolution limited (> 1000 Å) in the distorted-hexagonal phase, but decrease continuously as the temperature is lowered below $T = 970$ K. Further, the transverse line shapes below $T = 970$ K clearly display hysteresis for increasing and decreasing temperatures, and for different cooling rates.[8] The observation of hysteresis raises important questions about the possibility of attaining true thermodynamic equilibrium in the rotated, distorted-hexagonal phase. At all temperatures, the vibrational amplitude normal to the surface in the top few layers is enhanced above the bulk value, as determined from reflectivity measurements.[7–9] Figure 2(c) shows a schematic real-space view of the rotated, distorted-hexagonal phase.

In the following, we amplify certain aspects of these three phases in more detail. A complete discussion may be found in Refs. 7–9.

II. DISTORTED-HEXAGONAL UNIT CELL

Figure 3 shows the results of two typical glancing incidence scans through the putative hexagonal reciprocal lattice at room temperature, plotted on a logarithmic scale. The paths (a) and (b) traversed through reciprocal space are shown inset in the top panel. The index H in the figure is the first component of $(H, K, L)c$, expressed in cubic units. Because the substrate has square symmetry, the surface has two equivalent domains related by a 90° rotation of the sample about the cubic [001] direction. In the experiments reported here, both domains yielded identical results, and therefore only one was examined in detail.

Shown in the top panel of Fig. 3 is the result of a scan from the origin in-plane through the $(1, 1, 0.07)c$ substrate peak, and beyond. The strongest peaks visible are the principal hexagonal peak at $(1, 0)h = (H, K, L)c = (1.206, 1.206, 0.07)c$ and the substrate peak at $(1, 1, 0.07)c$ (see Fig. 1). From this (and later high-resolution measurements) we conclude that, to within our resolution, the overlayer is weakly incommensurate (in-plane) with respect to the bulk. The magnitude of the difference between these two is the incommensurability $\delta = 0.206 \pm 0.001\sqrt{2}c^*$ along the bulk [110] direction. It is worth remarking that all the intensity at the hexagonal peaks arises from the surface reconstruction. In contrast, contributions to the scattering at substrate peaks arise from layers lying within about one penetration depth—several hundred angstroms for these incident and exit angles. Typical count rates for the principal hexagonal peak, absent the analyzing crystal, were about 10 000 per second on a background of < 1 per second. The radial full width at half-maximum (FWHM) of the principal hexagonal peak determined using an analyzing crystal was about $(2 \times 10^{-3})c^*$, which corresponds to an in-plane correlation length ($= \pi/\text{FWHM}$) of about 1000 Å. This length is to be compared with the several-thousand-angstrom single-step dimension determined by reflectivity methods for this sample.[6,9] Evidently, the in-plane crystalline order extends over a domain of length comparable to a typical step dimension at room temperature. Higher harmonics of the principal hexagonal peak, which are separated from it by integer multiples of the incommensurability δ, are visible at $H(=K) = 0.794c^*$, $1.412c^*$, and $1.794c^*$. We do not understand the origin of the weak scattering around the substrate peak at $(1, 1, 0.07)c^*$. It reappeared, although considerably weaker, in subsequent scans.

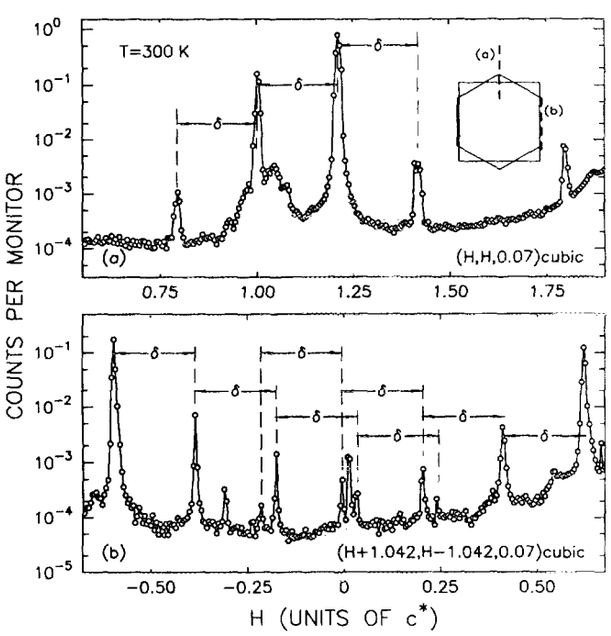

FIG. 3. Upper: scan through $(1, 1, 0.07)c$ and $(1, 0)h$. Lower: scan through $(0,1)h$ and $(1, 1)h$. Inset: the paths traversed through reciprocal space in each case. The index is H in cubic reciprocal-lattice units. Solid lines are the results of fits to the data.

In the lower panel of Fig. 3 the result of a scan taken at $T = 300$ K is shown, joining the $(0, 1)h$ hexagonal peak on the left to the $(1, 1)h$ hexagonal peak on the right. Four harmonics of each, one separated from the next by the incommensurability δ, are visible. The peak at the center of the scan, near $H = 0$, is the tail of the substrate peak at $(1, -1, 0.07)c$ [see Fig. 1(c)]. It is manifest from the splitting of the higher harmonics in Fig. 3(b) that the overlayer is incommensurate with the substrate. Because it never reappeared in subsequent, otherwise identical scans, we believe that the peak at $H = -0.3$ is spurious. Comparable intensities and full widths were obtained at the $(1, 1)h$ and $(0, 1)h$ hexagonal peaks, as were obtained at the $(1, 0)h$.

In this way, all the in-plane peaks we have observed (see Fig. 1) may be indexed as sums and differences of the hexagonal peaks at $(1, 0)h$, and the substrate peak at $(1, 1, 0.07,)c$. Equivalently, the in-plane peaks maybe indexed as sums and differences of the hexagonal peaks and the incommensurability δ. It follows that the hexagonal surface layer is modulated by the substrate potential (and vice versa), which leads to mixing of the surface and bulk periodicities in the x-ray diffraction pattern.

Before discussing the reflectivity, we note the mean lattice constants of the surface-layer unit cell. From high-resolution scans of the incommensurability of the $(1, 0)h$, $(0, 1)h$, and $(1, 2)h$ reflections, we have determined the average lattice parameters of the hexagonal unit cell to be $a = 2.763 \pm 0.002$ Å, $b = 2.766 \pm 0.002$ Å, and $\gamma = 120.03 \pm 0.1$° at room temperature. The corresponding quantities for bulk cubic (111) planes are $a = 2.885$ Å, $b = 2.885$ Å, and $\gamma = 120$°. This implies that the overlayer is contracted by 4.3% in the $[1\bar{1}0]$ direction and by 4.2% in the [110] direction. The relative orientation of the hexagonal unit cell and the cubic unit cell is established by the collinearity of the $(1, 0)h = (1.206, 1.206, 0.07)c$ and $(1, 1, 0.07)c$ reflections [See Fig. 1(b)]. It is important to note that with these average lattice constants the overlayer is hexagonal, to within the experimental error, and incommensurate with the square substrate in both directions along the surface.

III. SPECULAR AND NON-SPECULAR REFLECTIVITY

Figure 4 displays the measured absolute reflectivity as a function of $L = Q_z c/2\pi$ at a temperature of 1100 K, for several in-plane wave vectors. Because the data extend over a large range to $Q_z \cong 5$ A^{-1}, they are particularly sensitive to atomic coordinates perpendicular to the surface, and allow detailed modeling of the surface structure. Each point represents the integrated intensity obtained in a transverse scan.[6,9] The specular reflectivity is plotted in Fig. 4, curve (a). As has been discussed previously,[6,9] the line-shape asymmetry about the Bragg peak is a clear signature of a top-layer expansion [$d_{01} = 1.19 \times (c/2)$]. Figure 4, curves (e) and (f), show the nonspecular reflectivity at the principal hexagonal wave vectors, $(1, 0)h$ and $(0, 1)h$. Qualitatively, the Q_z dependence follows the $(\sin \alpha)^{-2}$ behavior expected from Eq. (1) for a hexagonal monolayer. The small deviations are related to the surface corrugation and small displacements parallel to [1$\bar{1}$0].[9] Figure 4, curve (b), shows the reflectivity at the modulation wave vector (δ, δ, L). This profile shows a significant increase from $L = 1$ to 2 and a line-shape asymmetry about $L = 2$, reminiscent of the specular reflectivity. The simplest explanation of the similarity of the Q_z dependence of the reflectivity at an incommensurate in-plane wave vector (δ, δ) to the specular reflectivity is that several layers participate in the reconstruction; that is, are modulated. The absence of significant increase near $L = 0$ of the nonspecular reflectivity along (δ, δ, L) further suggests that the modulation is a surface corrugation with atomic displacements normal to the surface. A schematic view of the inferred multilayer buckling is shown in Figs. 2(b) and 2(c). Similar remarks apply also to the nonspecular reflectivities along $(1, 1, L)$ and $(1 - \delta, 1 - \delta, L)$ shown in Figs. 4(c) and 4(d), respectively.

We have also fitted the reflectivity using Eq. (1), assuming a locally commensurate (5×1) structure. While this motif is not repeated periodically, nevertheless, such a simple model for $\rho_Q(n)$ provides an excellent description of the data (solid lines in Fig. 4). The parameters used were a layer-dependent sinusoidal corrugation amplitude for each layer (ζ_0–ζ_5), the layer spacings (d_{01}, d_{12}), and a layer-dependent vibrational amplitude normal to the surface (σ_0–σ_3). A detailed expression for $\rho_Q(n)$, including these parameters, is given in Ref. 9. Allowing parameters for additional layers to vary did not improve the quality of the fits. Fitting all the profiles of Fig. 4 together confirms the expectations outlined above and describes in detail the data of Fig. 4, curves (c) and (d). We find that the dependence of ζ_n on the distance from the surface (z_n) is well described by $\zeta_n = \zeta_0 \exp(-z_n/\lambda)$ with $\zeta_0 = 0.28 \pm 0.02$ Å (0.56 Å peak to peak), in reasonable agreement with the He atom scattering results of Ref. 5, and $\lambda = 3.3 \pm 0.6$ Å. Simple elasticity theory leads one to expect that λ be of the order of the modulation wavelength divided by 2π, i.e., 2.29 Å. The surface-normal vibrational amplitudes approach the bulk value for large n but are enhanced near the surface (Table I). As for the interlayer spacings, only d_{01} is measurably different from the bulk layer spacing.

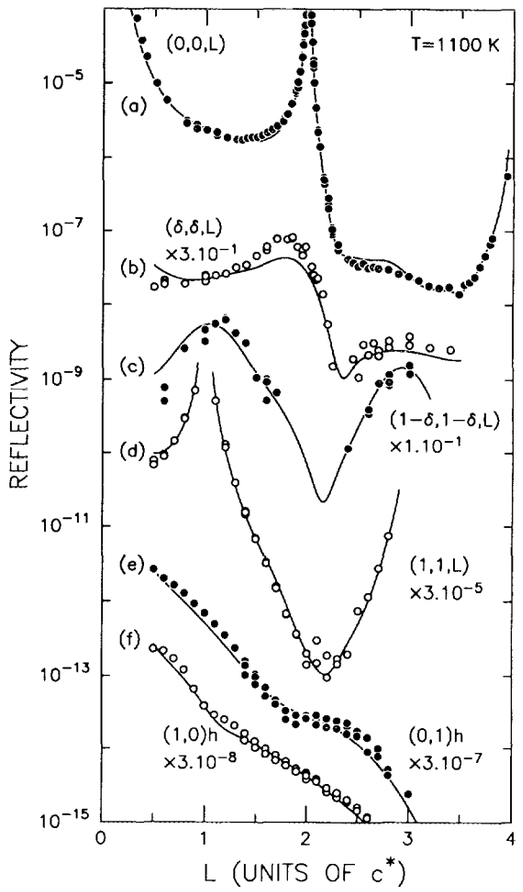

FIG. 4. Absolute reflectivity of Au(001) at 1100 K for various different in-plane wave vector transfers (τ_x, τ_y): curve (a), (0, 0), specular reflectivity; curve (b), (δ, δ); curve (c), $(1 - \delta, 1 - \delta)$; curve (d), (1, 1); curve (e), $(0, 1)h$ and curve (f), $(1, 0)h$.

IV. ROTATED DOMAINS

As the temperature is decreased below $T = 970$ K, there is a discontinuous rotational transition in which hexagonal do-

TABLE I. The rms, surface-normal vibrational amplitude for the nth layer (σ_n) vs temperature. The surface layer corresponds to $n = 0$.

Temperature (K)	σ_0 (Å)	σ_1 (Å)	σ_2 (Å)	σ_3 (Å)	σ_4 (Å)	σ_5 (Å)	Bulk
300	0.19 ± 0.02	0.17	0.09	0.09	0.09	0.09	0.09
1100	0.32	0.26	0.22	0.19	0.17	0.17	0.17
1200	0.44 ± 0.04	0.34	0.29	0.24	0.21	0.19	0.18

mains rotate to positive and negative angles. Typical transverse scans (ω-rocking curves) across the hexagonal rods at $(1, 0)h$, $(2, 0)h$, and $(1, 1)h$ and across the substrate rod at $(1, 1, 0.07)c$ are shown in Fig. 5, plotted on a logarithmic intensity scale, for $T = 650$ K. In each of the scans through a hexagonal rod, there is a peak at the center with $\omega = 0°$, and two adjacent peaks with $\omega = \pm 0.81 \pm 0.05°$. No additional peaks are observed in the scan through the substrate rod at $(1, 1, 0.07)c$. The solid lines in the figure show the results of fitting the data to Lorentzian line shapes, which proved superior to Gaussian line shapes for this analysis. While the fits clearly deviate in the wings, they are excellent in the neighborhood of the maxima, and give reliable values for the angular widths, peak positions, and peak intensities. When the data are plotted on a linear scale, the intensity is seen to be sharply peaked at $\omega = 0°$, $\pm 0.81°$, and the deviations are not noticeable.

The absence of additional peaks around the substrate peak at $(1, 1, 0.07)c$ unambiguously identifies the peaks at $\omega = \pm 0.81°$ with the surface layer. The fact that the angular splitting is the same at $(2, 0)h$ as it is at each comer of the hexagonal cell then establishes that the additional peaks arise from rotated, hexagonal domains [see Fig. 1(c)]. According to this interpretation, the rotation angle is just the value of ω. Because the three peaks have approximately equal intensities, we may infer that the populations across the surface of the unrotated and rotated hexagonal domains are sharply peaked at $\omega = 0°$ and $\pm 0.81°$ and are roughly comparable in number at $T = 650$ K. A schematic real space view of a rotated domain is shown in Fig. 2(c). The rotational transition of the Au(001) surface is discussed in more detail in Ref. 8.

V. DISORDERED PHASE

At $T = 1170$ K, all the scattering at the in-plane hexagonal wave vectors, and of their satellites, abruptly disappears. This is illustrated in Fig. 6, which shows the sum of the integrated intensities of the rotated and unrotated components of the hexagonal peak at $(1, 0)h$ plotted versus temperature. As may be seen, the integrated intensity is approximately constant below $T = 1000$ K, but vanishes over a range of ~ 10 K, consistent with a first-order transition to an unreconstructed or disordered surface layer. [The diffraction pattern observed in the high-temperature phase is shown in Fig. 1(a).] In addition, the reflectivity near the $(110)c$-position decreases by nearly a factor of 100 as the temperature is increased above 1170 K. In order to explore the hexagonal disorder transition at high temperatures, we performed measurements of the specular and nonspecular reflectivity near 1170 K. Examples are shown in Fig. 7, at 1200 K and, for comparison, at 1100 K in the distorted-hexagonal phase. Evidently, there is a dramatic change in going through the transition. In contrast, there is no change in the transverse line shape or position.[9] One may characterize the specular reflectivity as corresponding to an unreconstructed surface with enhanced surface-normal vibrational amplitudes. However, it is impossible on this basis alone to understand the decrease of the $(1, 1, L)$ reflectivity at small L from 1100 to 1200 K. On the other hand, the reflectivity

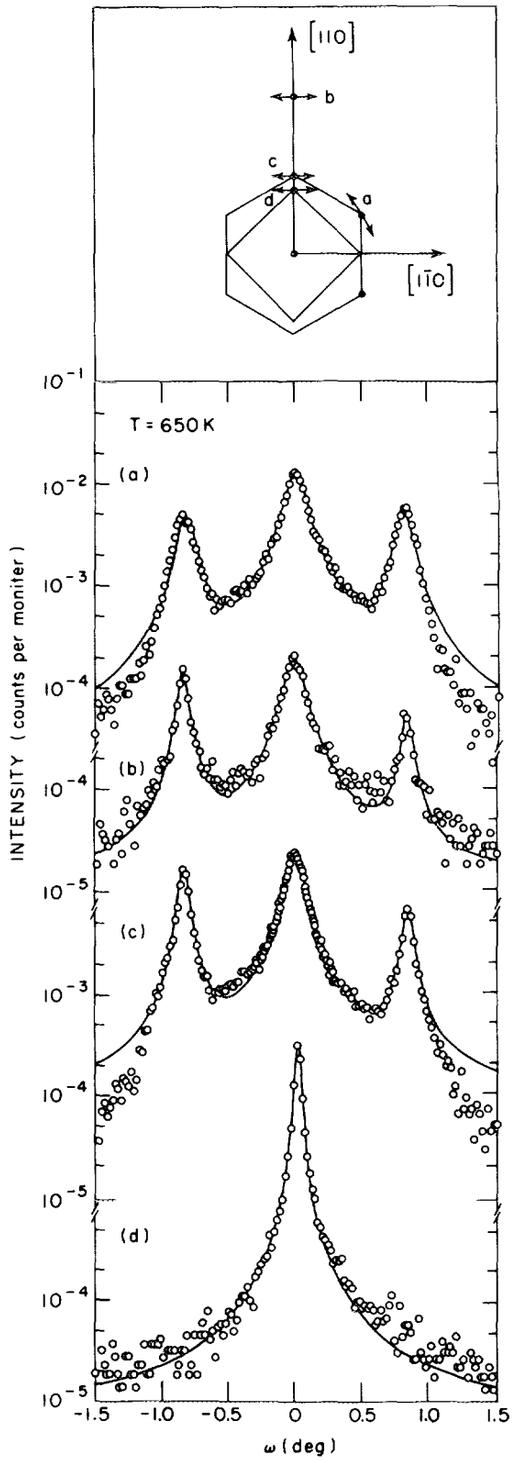

FIG. 5. Transverse scans through the surface $(1, 0)h$, $(2, 0)h$, $(1, 1)h$, and bulk $(1, 1, 0.07)c$ peaks at $T = 650$ K. The paths transversed through reciprocal space are indicated in the upper part of the figure. In (a)–(c) the peak at the center of the scan is the unrotated peak. The peaks split to the right and left are the rotated peaks. Solid lines are the results of Lorentzian fits.

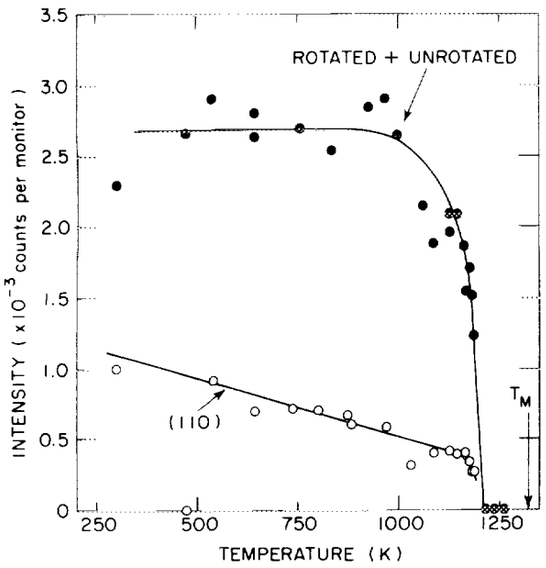

FIG. 6. Solid circles: the sum of the integrated intensities of the rotated and unrotated components of the hexagonal peak at $(1, 0)h$ for decreasing temperature. Open circles: the integrated intensity of the substrate peak at (1, 1, 0.07)c versus temperature. In both cases the integrated intensities were calculated from the Lorentzian fits to the peaks amplitudes.

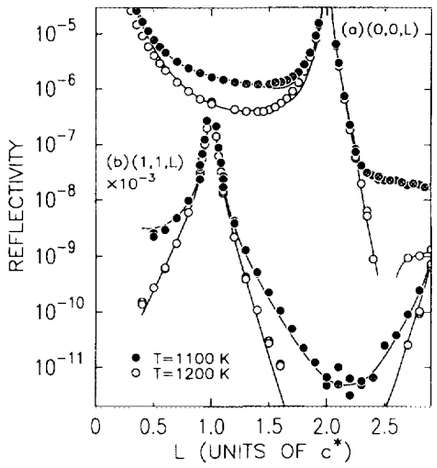

FIG. 7. (a) specular and (b) nonspecular reflectivity at 1100 K (closed circles) in the distorted-hexagonal phase and at 1200 K in the disordered phase (open circles). Solid lines are fits to the reflectivity discussed in the text.

from a gradual interface is invariably less than that from a sharp interface.[9] Thus these data imply that at high temperatures the in-plane (1, 1, 0) cubic density wave decays as the surface is approached from the bulk. This, in fact, is the behavior expected if the surface undergoes a melting transition.[14,15] To model the data of Fig. 7, we have chosen the following form for $\rho_Q(n)$ [G = (110) cubic] in the disordered phase.

$$\rho_G(n)/\rho_G(\infty) = 1 - 1/[1 + e^{\kappa l}\sinh(\kappa n + S)], \qquad (2)$$

with $S = e^{\kappa l}[1/(1 - e^{-\kappa l}) - 1]$. Other parametrizations are also possible.[9] According to Eq. (2), the density-wave profile is described by two parameters: the width of the interface κ^{-1} and the thickness of the disordered, surface layer (1). The solid lines of Fig. 7 are the results of fits with a model, which allows a surface-normal vibrational amplitude for each layer near the surface and which characterizes $\rho_Q(n)$ via Eq. (2); the density of the surface layer was fixed equal to that of the bulk planes. The resultant values of κ^{-1} and δ are 2.9 ± 0.4 A and 3.2 ± 1.2 Å, respectively, and indicate that the surface may be described as one or two disordered layers at these temperatures [see Fig. 2(a)] The best-fit value of d_{01} corresponds to an 8.5% expansion. The vibrational amplitudes, determined by the specular reflectivity, are given in Table I. Since the surface-normal vibrational amplitudes are less than the (001)-layer spacing, the layer order is still well established right to the surface. Surface disordering transitions have previously been observed on Pb(110).[16]

In summary, we have presented a detailed x-ray diffraction study of the Au(001) surface. This has allowed a definitive characterization of the reconstruction. We have discovered a rotational transition, which is not naturally described by current theories.[8] Finally, we have presented evidence for a surface-disordering transition. Future experiments will study the behavior nearer the triple point and especially the thickness of the disordered layer.[14,15] It remains to be determined whether surface disordering in this case is a consequence of the instability, which leads to the reconstruction, or whether it is generic to fcc(001) metal surfaces.

ACKNOWLEDGMENTS

We would particularly like to thank G. Ownby for technical assistance. Work at MIT is supported by the NSF (Grants No. DMR-8806591 and No. DMR-8719217), work at BNL by the DOE (Contract No. DE-AC0276CH00016), and at the ORNL by the Division of Materials Sciences, US DOE under Contract No. DE-AC05-84OR21400 with Martin Marietta Energy Systems Inc. X20 is supported by the NSF Materials Research Laboratory Program MIT (Grant No. DMR-8719217) and by IBM.

[1] D. M. Zehner, B. R. Appleton, T. S. Noggle, J. W. Miller, J. H. Barret, L. A. Jenkins, and E. Schow, III, J. Vac. Sci. Technol. **12**, 454 (1975).
[2] M. A. Van Hove, R. J. Koestner, P. C. Stair, J. B. Biberian, L. L. Kesmodel, I. Bartos, and G. A. Somorjai, Surf. Sci. **103**, 189 (1981).
[3] G. Binnig, H. Rohrer, Ch. Gerber, and E. Stoff, Surf. Sci. **144**, 321 (1984).
[4] K. Yamazaki, K. Takayanagi, Y. Tanishiro, and K. Yagi, Surf. Sci. **199**, 595 (1988).
[5] S. K. Rieder, T. Engel, R. H. Swendsen, and M. Manninen, Surf. Sci. **127**, 223 (1983).
[6] D. Gibbs, B. M. Ocko, D. M. Zehner, and S. G. J. Mochrie, Phys. Rev. B **38**, 7303 (1988).
[7] S. G. J. Mochrie, D. M. Zehner, B. M. Ocko, and D. Gibbs, Phys. Rev. Lett. **64**, 2925 (1990).
[8] D. Gibbs, B. M. Ocko, D. M. Zehner, and S. G. J. Mochrie, Phys. Rev. B **42**, 7330 (1990).
[9] B. M. Ocko, D. Gibbs, K. Huang, D. M. Zehner, and S. G. J. Mochrie, Phys. Rev. B (submitted).

[10] I. K. Robinson, Phys. Rev. B **33**, 3830 (1986); S. R. Andrews and R. A. Cowley, J. Phys. C **18**, 6427 (1985); A. M. Afanaslev, P. A. Aleksandrov, S. S. Fanchenko, V. A. Chaplanov, and S. S. Yakimov, Acta Crystallogr. Sect. A **42**, 116 (1986).
[11] H. Hong, C. J. Peters, A. Mak, R. J. Birgeneau, P. M. Horn, and H. Suematsu, Phys. Rev. B **40**, 4797 (1989).
[12] K. L. D'Amico, D. E. Moncton, E. D. Specht, R. J. Birgeneau, S. E. Nagler, and P. M. Horn, Phys. Rev. Lett. **53**, 2250 (1984); K. L. D'Amico, J. Bohr, D. E. Moncton, and D. Gibbs, Phys. Rev. B **41**, 4368 (1990).
[13] E. D. Specht, A. Mak, C. Peters, M. Sutton, R. J. Birgeneau, K. L. D'Amico, D. E. Moncton, S. E. Nagler, and P. M. Horn, Z. Phys. B **69**, 347 (1987).
[14] R. Lipowsky, V. Breuer, K. C. Prince, and H. P. Bonzel, Phys. Rev. Lett. **62**, 913 (1989).
[15] H. Lowen, T. Beier, and H. Wagner, Europhys Lett. **9**, 701 (1989).
[16] J. W. M. Frenken and J. F. Vanderveen, Phys. Rev. Lett. **54**, 134 (1985); J. W. M. Frenken, P. M. J. Maree, and J. F. Vanderveen, Phys. Rev. B **64**, 7506 (1986); B. Pluis, T. N. Taylor, D. Frankel, and J. F. Vanderveen, *ibid.* **40**, 1353 (1989).